NASA/TP-2006-213719

NASA Radiation Track Image GUI for Assessing Space Radiation Biological Effects

Artem L. Ponomarev
NASA Lyndon B. Johnson Space Center
Houston, Texas

Francis A. Cucinotta
NASA Lyndon B. Johnson Space Center
Houston, Texas

May 2006

THE NASA STI PROGRAM OFFICE . . . IN PROFILE

Since its founding, NASA has been dedicated to the advancement of aeronautics and space science. The NASA Scientific and Technical Information (STI) Program Office plays a key part in helping NASA maintain this important role.

The NASA STI Program Office is operated by Langley Research Center, the lead center for NASA's scientific and technical information. The NASA STI Program Office provides access to the NASA STI Database, the largest collection of aeronautical and space science STI in the world. The Program Office is also NASA's institutional mechanism for disseminating the results of its research and development activities. These results are published by NASA in the NASA STI Report Series, which includes the following report types:

- TECHNICAL PUBLICATION. Reports of completed research or a major significant phase of research that present the results of NASA programs and include extensive data or theoretical analysis. Includes compilations of significant scientific and technical data and information deemed to be of continuing reference value. NASA's counterpart of peer-reviewed formal professional papers but has less stringent limitations on manuscript length and extent of graphic presentations.

- TECHNICAL MEMORANDUM. Scientific and technical findings that are preliminary or of specialized interest, e.g., quick release reports, working papers, and bibliographies that contain minimal annotation. Does not contain extensive analysis.

- CONTRACTOR REPORT. Scientific and technical findings by NASA-sponsored contractors and grantees.

- CONFERENCE PUBLICATION. Collected papers from scientific and technical conferences, symposia, seminars, or other meetings sponsored or cosponsored by NASA.

- SPECIAL PUBLICATION. Scientific, technical, or historical information from NASA programs, projects, and mission, often concerned with subjects having substantial public interest.

- TECHNICAL TRANSLATION English-language translations of foreign scientific and technical material pertinent to NASA's mission.

Specialized services that complement the STI Program Office's diverse offerings include creating custom thesauri, building customized databases, organizing and publishing research results . . . even providing videos.

For more information about the NASA STI Program Office, see the following:

- Access the NASA STI Program Home Page at http://www.sti.nasa.gov

- E-mail your question via the Internet to help@sti.nasa.gov

- Fax your question to the NASA Access Help Desk at (301) 621-0134

- Telephone the NASA Access Help Desk at (301) 621-0390

- Write to:
  NASA Access Help Desk
  NASA Center for AeroSpace Information
  7121 Standard
  Hanover, MD 21076-1320

NASA/TP-2006-213719

NASA Radiation Track Image GUI for Assessing Space Radiation Biological Effects

Artem L. Ponomarev
NASA Lyndon B. Johnson Space Center
Houston, Texas

Francis A. Cucinotta
NASA Lyndon B. Johnson Space Center
Houston, Texas

May 2006

Available from:

NASA Center for AeroSpace Information
7121 Standard Drive
Hanover, MD 21076-1320
301-621-0390

National Technical Information Service
5285 Port Royal Road
Springfield, VA 22161
703-605-6000

This report is also available in electronic form at http://ston.jsc.nasa.gov/collections/TRS/

Contents

Tables

Figures

Acronyms

bp	base pair
CPU	central processing unit
DNA	deoxyribonucleic acid
DSB	DNA double-strand break
Gbp	giga base pair
GCR	galactic cosmic rays
GUI	graphics user interface
HZE	high-charge high-energy
kbp	kilo base pair
LET	linear energy transfer
Mbp	mega base pair
MLS	multi-loop-subcompartment model of DNA loops on the Mbp-Gbp scale
OpenGL	open graphics library
PFGE	pulsed-filed gel electrophoresis experiment
RBE	radio-biological efficiency
RLC	randomly located cluster
RW	random walk
SPE	solar particle event
3D	three-dimensional
USRA	Universities for Space Research Association

Abstract

The high-charge high-energy (HZE) ion components of the galactic cosmic rays present unique challenges to biological systems in comparison to terrestrial forms of radiations. We present a deoxyribonucleic acid (DNA) breakage model to visualize and analyze the impact of chromatin domains and DNA loops on clustering of DNA damage from X-rays, protons, and HZE ions. Our model of DNA breakage is based on a stochastic process of DNA double-strand break (DSB) formation that includes the amorphous model of the radiation track and a polymer model of DNA packed in the cell nucleus. Our model is a Monte-Carlo simulation based on a randomly located DSB cluster formalism that accommodates high- and low-linear energy transfer radiations. We demonstrate that HZE ions have a strong impact on DSB clustering, both along the chromosome length and in the nucleus volume. The effects of chromosomal domains and DNA loops on the DSB fragment-size distribution and the spatial distribution of DSB in the nucleus were studied. We compare our model predictions with the spatial distribution of DSB obtained from experiments. The implications of our model predictions for radiation protection will be discussed.

1. Introduction

ONE of the main concerns for long-term deep space missions is health risks associated with prolonged exposure to proton and high-charge high-energy (HZE) components of the galactic cosmic rays (GCR) and solar radiation in space. It is known that an astronaut on a six-month journey to Mars, which is the time required with conventional propulsion, would be exposed to about 0.3 Sieverts (1 Sievert = 1 Gray = 1 Joule/kg = 100 rad = 100 rems for X rays, but is equal to Q×1 Gray = 100 rems = Q×100 rads for high-linear energy transfer (LET) radiation, where Q is the biological quality of radiation; Q > 1 for high-LET), or even to 0.6 Sieverts on a round-trip (Cucinotta *et al*., 2005). Eighteen months on the surface (if it takes that long to get there, you might as well stay for a while) would bring another 0.4 Sieverts, for a total exposure of 1 Sievert. Limits set by NASA vary with age and gender ranging from 0.5 to 2 Sieverts.. During a 3-year mission to Mars at solar minimum (worst case for the GCR exposure), 46% of cells might be hit by an HZE particle (with the electric charge Z > +15), with 13% hit by an iron particle (Z = +26). Hit frequencies are 4–8 times lower for nuclei of cells. The cell nucleus would also be traversed by a proton twice a week, and an α-particle once a month (Badhwar *et al*., 2002; NCRP report 98; Townsend *et al*., 1992; Cucinotta *et al*., 1998b). Particle fluences from GCR may be more relevant than absorbed radiation doses, which will be a few tens of cGy, to the human body. This is because the radiation effects measured at short times after fractionated doses of 100 cGy or higher, which correspond to several hits per cell, may not accurately predict astronaut risk because of deoxyribonucleic acid (DNA) repair. Repair and adaptation mechanisms (Rothkamm & Löbrich, 2003), which can counteract effects of particles delivered chronically, may be overwhelmed by the delivery of radiation as an acute dose from one fraction. It is also important to remember that other conditions during spaceflight may modify responses to HZE radiation.

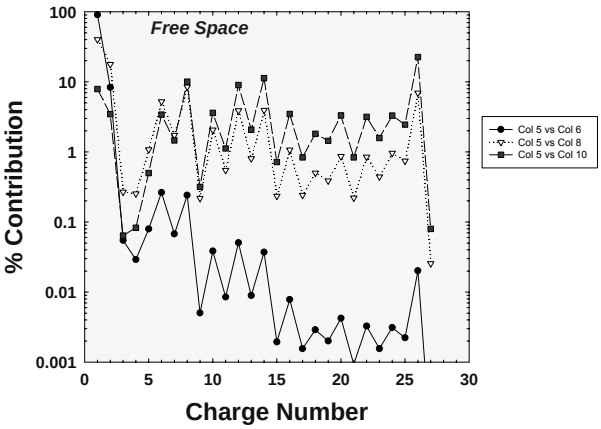

Figure 1. GCR charge contribution.

GCRs are the major radiation source in outer space, and these are composed of H (85%), He (13%), and HZE particles (1%). The relative abundance and ionizing power of the even-numbered HZE particles in GCR is well studied (Report LBNL-40278). Although the fluence of HZE particles in GCR is low, the high charge of these particles makes them particularly damaging (Fig. 1). Because of its relative abundance, and charge of Z = +26, Fe is a major concern among the various HZE particles encountered. Although C, O, B, Li, N, and Be particles are less highly charged, their abundance indicates they must also be considered.

Some knowledge about exposure to HZE particles in outer space has already been gained, as the HZE dose rate during the Apollo 17 flight was calculated to be 0.12 μGy per hour, or about 1.05 mGy per year for HZE particle irradiation. Ignoring solar particle events (SPEs), the total dose of radiation during a 3-year mission is about 0.3 Gy,

mostly due to protons. It has been estimated that during a Mars mission, annual exposure from GCR would be between 0.15 Sv/year at solar maximum and 0.58 Sv/year at solar minimum. It has been estimated that SPE exposure (from electrons and protons as well as other secondary radiation induced by them) may contribute about another 0.3 Sv/year, or almost 1 Sv on a 3-year Mars mission, although the exposure rate due to an SPE could increase 100- to 1000-fold during brief intervals (up to several days). However, in contrast to GCR, shielding can effectively mitigate SPE doses with their energies and ranges in materials being much lower compared to GCR.

Energy deposition from GCR is largely confined to a thin cylinder of tissue that receives a high local dose, especially at the end of the particle range, which is the depth of tissue penetration (Turner *et al.*, 2002). One can calculate that for a 1-GeV/u ^{56}Fe particle, the average dose to a nucleus that would be traversed near the nucleus center, as recent data by our model show, would be about 12 cGy. Furthermore, the effect of ionizing radiation on cells and, ultimately, tissues originates primarily from damage to DNA; and the complex ways in which particular types of radiation interact with matter and break and/or otherwise alter DNA structures control the potential consequences of radiation, modulated by the ability of cells to repair damage. The passage of an HZE particle through the cell nucleus should cause multiple, intense, and essentially instantaneous ionization events that induce complex patterns of DNA damage, sometimes irreparable. Little is known about the effects of charged particles at the cellular and molecular level in mitotic cells. Mitochondrial as well as nuclear DNA can be a radiobiological target. Since the mitochondrial electron transport chain is the main endogenous source of reactive oxygen species that causes oxidative stress, damage to mitochondrial DNA can be particularly relevant during spaceflight. Mitochondria have multiple copies of their genome and even possess DNA repair enzymes. However, the studies of the effects of HZE radiation in this area are insufficient.

The radiation damage of DNA is crucial to understanding the effect of radiation on an astronaut's body (Goodhead, 1995). DNA is a set of long molecules comprising 46 human chromosomes in a normal diploid genome. The female genome is slightly longer because of the double X chromosome, which is much larger than the Y chromosome. We have developed computer models, and related codes, as well as visualization software of damage to DNA from charged particle tracks. For the current analysis we simulated the male genome with XY chromosomes. Our code can easily allow for the double X chromosome. The genomic size is typically measured in the number of base pairs (bps) of the well-known double-helix molecule, or its derivatives, kilo base pairs (kbps) and mega base pairs (Mbps). The genomic size is proportional to the molecular weight of the chromosomes, even though it far exceeds the molecular weight of the bases, containing the genomic information, because chromatin, or the fiber that the chromosomes are made of, is a complex collection of structural proteins, mostly (Rogakou *et al*., 1998) histones (Fig. 2). The total length, or molecular weight, of the human genome, is about 3.2 Gbps (giga base pairs).

Radiation causes ionizations in cell water that leads to aggressive water radicals attacking DNA. One consequence of radiation is the loss of bases that have the genomic information (Taucher-Scholz, 2000). The loss of one base is called a single strand break. If two single-strand breaks occur within about 10–50 bp, a DSB is produced (Wu *et al*., 1996; Brenner & Ward, 1992). Although methods for measuring DNA damage have been developed over the years, it is still unclear how well damage can be measured at low doses because of the small regions or molecular sizes of the damaged regions of interests. The most common measurement is the pulsed-filed gel electrophoresis experiment (PFGE), where after special preparation of DNA and the use of an applied electric field, a collection of fragments produced by DSB is sorted by the molecular size and the DNA fragment distribution is measured. The number of fragments is almost precisely equal to the number of DSBs. The limitation of this experiment is that small fragments, as well as very large ones, cannot be detected. There are very few large fragments, so this number is not significant; but the number of small fragments is large and dependent on the radiation quality, and, thus, is an important consideration in determining the effects of space radiation. Here we report our novel method of accounting for missing fragment and leading to new estimates of DSB counts induced by radiations relevant to space environment. We also compare our approach to other approaches (Results section).

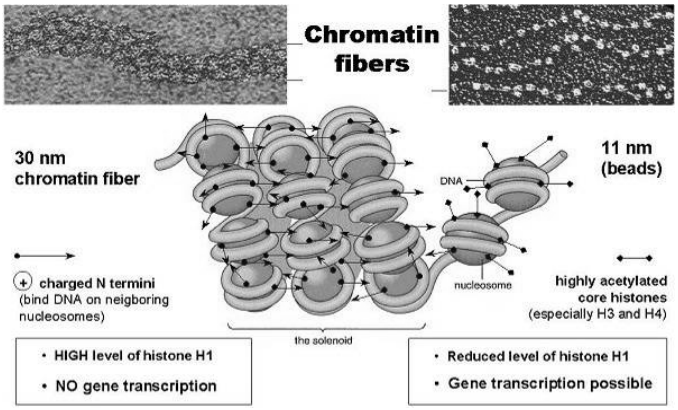

Figure 2. The high-order structure of DNA is shown on the level of chromatin fiber. The source for this is http://sgi.bls.umkc.edu/waterborg/chromat/chroma09.html. A piece of DNA depicted is about the size of one monomer that will be a building block for the whole genome in this work.

Another important consideration is the geometric statistics of DSB (Prise, 1997; Pinto *et al.*, 2004). The same total number of fragments may have a different relative number of smaller fragments. PFGE experiments report a number of smaller fragments in excess than one would expect if DSB were located randomly (Campa *et al.*, 2004) along chromosomes. This is believed to be the signature of the high-LET radiation, as well as the result of the particular properties of DNA organization in the cell nucleus. This phenomenon, called DSB clustering, is herein addressed by our model. The importance of these data is that DSB clustering indicates a higher severity of damage. A collection of closely located small fragments will more likely result in a permanent genomic damage, such as gross violation of DNA topology called chromosomal aberrations, and, as related to them, the loss of genomic information (gene deletions).

DNA damage can lead to cell death, which is not problematic for small doses during space missions. (In the majority of the brain tissues, however, cells do not replenish, so cell death is potentially dangerous.) More importantly, the accumulation of genomic damage can lead to late effects, such as cancer, through genomic instability and mutations.

At the NASA Johnson Space Center, we have developed a suite of numerical and mathematical tools to address the biophysical modeling of radiation, cells, and tissue. We will present here a brief description of methods used in the present work. First and foremost, we have developed precise physical models of radiation transfer through matter (Cucinotta *et al.* 1998a; Cucinotta *et al.* 1998b; Cucinotta *et al.*, 1995; Cucinotta *et al.*, 1999; Cucinotta *et al.*, 2000; Nikjoo *et al.*, 2002a; Nikjoo *et al.*, 2002b; Wilson *et al.*, 1987). These models address several types of radiations: low-LET, such as X rays, and gamma-rays; and high-LET radiation, which are primarily α-particles and heavier in mass, A, higher in charge, Z, and higher in energy E, HZE ions. LET is a significant parameter indicating the quality of radiation. Its meaning is simple; it is the energy in keV imparted to the matter (such as cell cytoplasm) per μm of the particle path. The more energy imparted per μm, the more biologically destructive the radiation is (for very high LET, there is a drop-off of the radiation efficiency due to overkill effect (NCRP report 98)). In the present analysis, we treat low-LET radiation as a homogenous field of radiation that does not have sharp peaks of deposited energy in small volumes. By high-LET radiation, we mean ions such as 1 GeV/a ^{56}Fe (an HZE ion), or α-particles, that have a sharp peak of deposited energy close to the track center. Some researchers argue that HZE ions are not strictly high-LET radiation due to their extensive penumbra (energy field at distances up to 50 μm from the track core), where energy is imparted by low-LET electrons (δ-rays). However, the track core (a narrow region around the particle trajectory) is high-LET, and it is more significant for the biological effects as our studies have shown.

We should distinguish between LET, which is an average measure of the energy loss along a track in z direction and integrated over the span of the track in x and y directions, and the track's energy profile in the x-, y-plane perpendicular to the particle direction. Often higher LET particles such as ^{56}Fe have a wider penumbra, or the extent of the energy field, than the particles with low LET. For instance, a 151-keV/μm ^{56}Fe ion deposits energy in the cylinder of up to 2×30 μm in diameter and more, while 40-keV/μm α-particles have a track confined to less than 0.1 μm of the high-energy deposition area, almost like a needle piercing cells. This field of energy surrounding impinging particles is simulated to a high precision by the program that we use in this work (Cucinotta *et al.*, 1999; Cucinotta *et al.,* 2000).

We have addressed the effect of radiation on cellular level, and designed a sophisticated model of DNA breakage in a cell (Ponomarev *et al.*, 2000). This model includes the track structure described above and a polymer model of chromosomes based on a random walk (RW) model for chromosomes (Fig. 3). This was a significant attempt to address the biological effects of radiation insult on cells based on our state-of-the-art knowledge of the underlying physical processes.

One of the main motivations for radiobiological research is to guide extrapolations of risk estimates from high to low radiation doses and associated dose-rates. By "low" we mean the dose-rate encountered in space, while the high dose-rate is of typical radiobiological experiments that have practical limitations on what dose and dose-rates conditions can be used. This is of importance for individuals environmentally exposed (e.g., from radon) or occupationally exposed (e.g., air-flight personnel and astronauts) to low- or high-LET radiations. For example, recent PFGE experiments (Löbrich *et al.*, 1996; Höglund *et al.*, 2000; Stenerlöw *et al.*, 2003; Belli *et al.,* 2000) provide DNA breakage yields at doses that are too high to be directly applicable to radiation risk predictions in humans. However, if a reliable model allowing extrapolation to low doses is available, high-dose data can provide the basis for useful information about DNA breakage yields at low doses. For low-LET radiation, the random-breakage model (Blöcher, 1990) is suitable for such a task.

The random-breakage model (Cook & Mortimer, 1991) that was used ubiquitously in the past is not adequate for high-LET radiation because it lacks mechanistic detail to allow for the pronounced clustering of DNA damage caused by the highly inhomogeneous energy profile of high-LET ion tracks. Specifically, the DNA is multiply folded during interphase; but, even on large scales, DNA loci, which are close to each other along the DNA contour, tend also, on av-

erage and neglecting fine-structure, to be spatially close to one another. With this geometry, a bias for ionizations to be close to each other in space at high LET produces a bias for DSBs to be close to each other along the DNA.

A new model, called NASARadiationTrackImage (Ponomarev *et al.*, 2000; Ponomarev *et al.,* 1999; Ponomarev *et al.*, 2001a), based on radiation track structure and large-scale chromatin geometry has been shown to predict the non-randomness of high-LET-induced DSB distributions within the genome. In the NASARadiationTrackImage model, ion track structure is simulated (Cucinotta *et al.*, 2000) and is superimposed on random-walk (Sachs *et al.*, 1995) chromatin geometry (Fig. 3a). To make the picture more realistic, we introduce chromatin loops (Fig. 3b), which are found in experiments revealing high-order DNA organization (Marco & Siggia, 1997). Ionizations due to a high-LET radiation track are spatially correlated, being predominantly near the line representing the center of the track (Fig. 3c) rather than spread randomly over a whole cell nucleus. This clustering of ionizations, which is determined by the type of incident particles, leads to correlations among DSBs along chromosomes as opposed to the mostly uncorrelated DSB produced by low-LET radiations. The advantage of this approach is that, since it is a generalization of the random-breakage model (suitable for X -rays, for example), it is easy to reduce the NASARadiationTrackImage model to the case with low LET (Ponomarev *et al.,* 2001b).

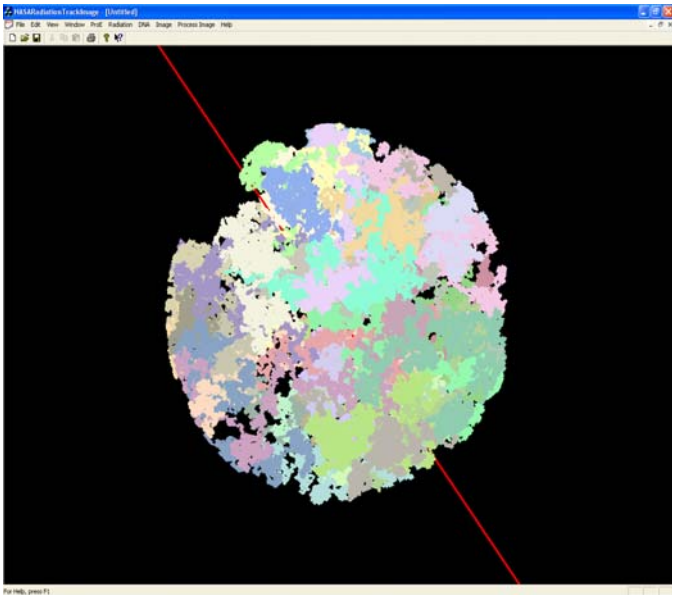

Figure 3a. The NASARadiationTrackImage graphics user interface (GUI) displaying one Monte-Carlo realization of RW (each chromosome given in a separate color), a track center (red line), and a round nucleus (the outline of the membrane is intuitively visible). Overlap between RWs may or may not be allowed. The software is able to simulate many tracks, an ellipsoidal nucleus, RW packed into defined chromosomal domains, certain impact parameter for the track, and a fixed fluence of particles. Each chromosome depicted here is a vast collection of dots (about 100,000) corresponding to monomers. Here, the scale of the whole nucleus individual dots is not discernable. The size of a chromosome corresponding to one dot is, however, about the size of a piece of DNA and the other accompanying molecules shown in Fig. 2.

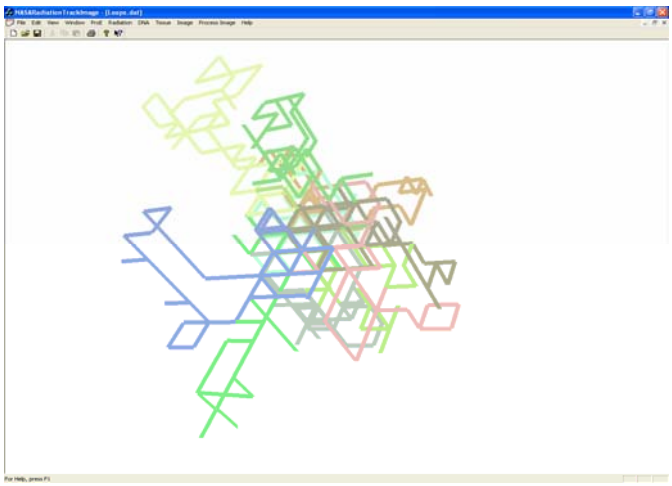

Figure 3b. A group of 10 loops is shown on a much smaller scale than in Panel A. One chromosome can be divided into 10–100 such structures, each structure containing 1320 kbps of genomic material. Loops in the model are produced by random walks that return to the origin.

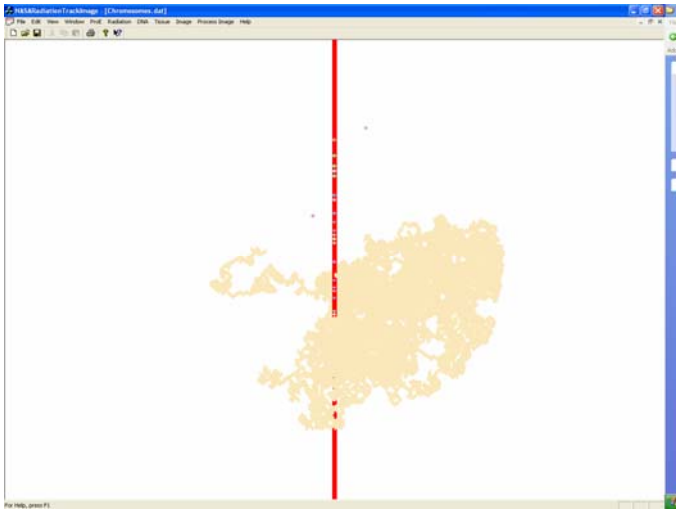

Figure 3c. A group of DSBs is shown, as well as an Fe track, and a chromosome #6 (other chromosomes are present but are not shown). DSBs are located predominantly along the track center. Due to an extended penumbra of the Fe ion track, some DSBs can form at a distance from the track center.

The proposed mechanistic approach predicts DSB fragment-size patterns in the genome over a very large range of fragment sizes (20 kbp–10 Mbp); this range has been successfully compared to the experimental data for a variety of situations (Ponomarev *et al.*, 2000; Ponomarev & Sachs, 1999; Sachs *et al.*, 1995; Sachs *et al.*, 1999) where distributions of DNA fragment sizes were measured after irradiation at LET≈80 keV/μm or more (Löbrich *et al.*, 1996; Höglund, *et al.*, 2000; Newman *et al.*, 1997).

The NASARadiationTrackImage model was previously formulated for a simple polymer model of DNA that had only RW for the chromosomal structure. In this work, we introduced the chromosomal domains and DNA loops as a more precise model of the high-order DNA organization in the cell nucleus. Our analysis of the impact of these structures on the fragment sizes is presented herein.

2. Methods

2.1. The application of randomly located clusters formalism

Our polymer model of DNA breakage is based on a more general (*i.e.*, than the random breakage model) randomly located clusters (RLCs) formalism (*i.e.*, the clusters of DSBs). The generality of the formalism is based on the fact that we do not need to know *a priori* the reason for DSB clustering, or the precise form of it, to infer breakage from many particles (high dose, or high fluence). The determination of the unknown function of clustered DSB can be delegated to a Monte-Carlo algorithm that we will describe below. Detailed descriptions of the RLC formalism and the Monte-Carlo algorithm employed in NASARadiationTrackImage are given in Ponomarev *et al.*, 2000, and in Sachs *et al.*, 1999, along with the validation and the benchmark of the algorithm. The fundamental ideas underlying the RLC formalism are that the one-track action can make a stochastic cluster of DSB along a chromosome; that different clusters on a chromosome, due to different tracks, are statistically independent; and that the location of DSB clusters in the genome, unlike the non-random location of DSB within one cluster, is random, or *Poisson* (hence the term RLCs).

The RLC formalism relates low-dose, one-track effects to high-dose, multi-track effects. Thus, only the one-track action needs to be simulated. This holds true for various radiations and various chromatin geometries, as long as the spatial distribution of incident ions traversing a certain area is random. It is assumed that there is no change of LET along the ion trajectory on the scale of a cell nucleus. The main result of the formalism is the inference of the multi-track action through the one-track action, as given by the following equation, stated for brevity for a genome with chromosomes of equal size S (the generalization to a more realistic genome is straightforward and is done computationally):

$$1 - R(s) = [1 - s/S]\, I(s) \exp\left[-\lambda \left[s + (M-1) \int_0^2 (1 - F(s'))\, ds' \right] \right] \tag{1}$$

where s = size (*i.e.*, genomic content in bp) of DNA; $R(s)$ = multi-track remaining-size distribution (Sachs *et al.*, 1999) for DNA fragments; $I(s)$ = unity for $s<S$ and zero otherwise (telomere cutoff (Laughton *et al.*, 2004)); λ = cluster intensity (Sachs *et al.*, 1999) = number of one-track DSB clusters per unit size of DNA (λ is proportional to the dose); M = average multiplicity (number of DSB) of an individual DSB cluster, induced by one track on one chromosome; and $F(s)$ = cumulative distribution for one-track DNA fragment sizes. $R(s)$, which completely characterizes the multi-track fragment size patterns (Sachs *et al.*, 1999), can be fit to a high-dose PFGE experiment. Thus Eq. (1) expresses full information about the multi-track response in terms of the dose parameter λ and of dose-independent, one-track quantities (M and $F(s)$). The proof of the equation is long but straightforward (Sachs *et al.*, 1999).

2.2. Monte-Carlo simulation of DNA damage

To calculate the one-track quantities M and $F(s)$, we introduce (except in the low-LET limit) specific models for the track and chromatin geometry. Our limit of resolution is set at 2 kbp for the smallest discernable feature of DNA (Figs. 1, 2) so that we can model the whole human genome. We consider the radial distribution of dose and the distribution of electron energies in the average track model (Cucinotta *et al.*, 1999; Kobetich & Katz, 1969). In this model, the distribution in the number of electrons ejected, n_i with energy, ω and solid angle, Ω produced by ion interactions with target atoms (*i.e.*, the double differential cross section for electron ejection) is combined with the

average transmission properties of electrons to obtain the spatial distribution of electron dose as a function of radial distance from the ion's path. The radial dose due to ionization is then described by (Kobetich & Katz, 1969) as:

$$D_\delta(t) = \frac{-1}{2\pi t} \sum_i \int d\Omega \int d\omega \, \frac{\partial}{\partial t}\left[E(t,\omega)\eta(t,\omega)\right] \frac{d^2 n_i}{d\omega d\Omega} \tag{2}$$

In Eq. (2), E is the residual energy of electrons after penetrating distance t, and $\eta(t,\omega)$ is the transmission probability that an electron with starting energy ω penetrates to a depth t. Reference (Cucinotta *et al.*, 1995) describes the input functions necessary to evaluate D in Eq. (2). Cross sections for electron production from protons are scaled to heavy ions using effective charge, which is expected to be accurate for high-energy ions. We follow (Brandt & Ritchie, 1974) for the dependence of the excitation term, $D_{exc}(t)$, on radial distance t in terms of the charge number Z and velocity with $d(\beta)=(\beta/2)\cdot hc/(2\pi\omega_r)$, where c is the speed of light, β is the relativistic velocity factor, and h is Planck's constant, and we use $\omega_r = 13$ eV for water. The constant C_{exc} is adjusted so that the model provides a good estimate of the LET (Cucinotta *et al.*, 1999).

$$D_{exc}(t) = C_{exc}(Z,\beta)\frac{\exp\left(-t/2d(\beta)\right)}{t^2} \tag{3}$$

This track structure model can be combined with a chromatin model to calculate the one-track action. In our NASARadiationTrackImage model, a random walk structure of chromatin is used as the basic DNA geometry. We divide a chromosome into a large number of evenly spaced monomers, with each monomer being the same size, typically ≈ 2 kbp. The spatial geometry of the chromatin is approximated by a random walk on a cubic lattice. Each lattice site is a node on the cubic lattice representing physical space; a monomer is located on one such site. The lower limit of resolution in the model corresponds to one monomer size, below which the structure of chromatin is not specified and DSB distributions are not modeled.

The track radial energy profile (Eq. (2)) is used to generate a stochastic process of DSB formation on human chromosomes, given by the probability Ψ of having at least one DSB on a monomer and given the monomer distance t from the track center in the XY plane (*i.e.*, in the plane perpendicular to the direction of radiation). This probability is given by (Ponomarev *et al.*, 2001a) as:

$$\Psi = 1 - e^{-\mathbf{Q}D(t)} \tag{4}$$

where $D(t)$ is the local dose (averaged over a small volume at the distance t from the track center). The quantity $\mathbf{Q}$ [Gy^{-1}] is a track efficiency parameter; it is the only adjustable parameter in our model and is defined more specifically in Eq. (5) below.

Despite large variations in $D(t)$ for the high-LET radiation, we found that in a typical simulation of the PFGE experiment $\mathbf{Q}D(t) \ll 1$ in any location within the cell nucleus, even at the sites close to the track center. In this approximation $\Psi \approx \mathbf{Q}D(t)$, which corresponds to the fact that if the dose in any small physical volume inside the cell nucleus increases, the number of DSBs produced there increases proportionately.

We can easily apply this formalism to the low-LET radiation by putting $D(t)$ to *const* (and equal to the dose of the experiment), Eq. (4) in this case translates into a *Poisson* statistics, or random breakage (Cook & Mortimer, 1991). The stochastic process generated by Eq. (4) can thus be used for both low- and high-LET radiations.

The algorithmic implementation of the RLC formalism can be expressed by the following two equations relating the experimental data and the formalism parameters:

$$\mathbf{Q} = DSB\_yield \times DNA\_size / N \tag{5}$$

$$\lambda = \mathbf{Q}D/M \tag{6}$$

In Eqs. (5, 6), D is the dose of the experiment in Gy; *DSB_yield* is the number of resolvable DSBs per unit dose and unit size, obtained in a PFGE assay; *DNA_size* is 140 Mbp, an average size for a human chromosome; and N is the

number of monomers (≈70,000) in an average chromosome. Another meaning of our adjustable parameter Q is the average number of resolvable DSBs per monomer per unit dose; that is, a local DSB yield. All radiochemistry involved in the creation of DSBs by ionizing radiation is encapsulated into the quantity Q, which will, of course, depend on track radiation efficiency but should not depend on dose (Eq. (4)). Eq. (6) shows how the dose determines λ, the average number of DSB clusters per chromosome, or the cluster intensity, which is also the number of tracks that interact with a chromosome, each track having produced at least one DSB. M is the average cluster multiplicity, or the average number of resolvable DSBs created on a chromosome in the one-track action (Sachs *et al.*, 1999; Ponomarev & Sachs, 1991). The RLC formalism relates the multi-track fragment-size distribution function that can be obtained analytically from Eq. (1) and the one-track action (Sachs *et al.*, 1999) that is simulated by our algorithm using Eqs. (4-6). Our model is validated by fitting the DNA fragment frequencies obtained with our algorithmic and theoretical approach to the experimental data.

Another justification of our approach to the prediction of DNA fragment sizes and the DSB yield is that the DSB yield is never directly measured in a PFGE assay: some approximations are used to infer its value (Löbrich *et al.*, 1996; Höglund *et al*., 2000; Radulescu *et al.*, 2004). Our model provides a systematic approach instead of implicit extrapolations that PFGE experimentalists do for small fragments and the DSB yield inferred from the number of fragments. We predict the DSB yield from Eq. (5), once the optimal value for Q is found by χ^2-fitting the model to the experimental data. The reason our DSB yield is more systematic is because it is based on a more detailed analysis of the track structure and the DNA geometry. We presented the χ^2-fitted Q values for a variety of experimental situations elsewhere (Ponomarev *et al.*, 2001a; Ponomarev *et al.*, 2001b). These values of Q can be used to predict the DNA fragmentation and DSB yields at any dose for any ion presented in Table I. The low dose extrapolation can be made with our model, and the DSB yield and DNA fragmentation can be predicted for a Microbeam experiment with a fixed number of particles per cell.

Table I. The intensity parameter Q of the stochastic process of DSB formation. The estimated values for the intensity of the stochastic process of DSB formation Q (Eq. 1) are shown in a variety of experimental situations. Data are grouped into dose intervals and are taken from different groups (based on the data from (Löbrich *et al.,* 1996)*; other entries based on the data from (Höglund *et al.,* 2000); newer data† are based on a model fit to (Radulescu *et al.,* 2004)). Some discrepancy between experimental groups was observed, e.g., Q=2.46×10^5 Gy^{-1} for (Löbrich *et al.,* 1996), and Q=1.7×10^5 Gy^{-1} for (Höglund *et al.,* 2000) for the same radiation (N ions at 80-97 keV/μm), and the same dose. Q is dose-independent and near LET-independent.

Q x10^5	Fe, 150 keV/μm	N, 80-97 keV/μm	N, 125 keV/μm	N, 175 keV/μm	N, 225 keV/μm	He, 40 keV/μm	^{60}Co-photons <0.5 keV/μm
150-200 Gy	3.71±0.01*	2.46*;1.70 ±0.01	1.81±0.01	1.43±0.01	1.41±0.01	1.83±0.01	1.2±0.01
100 Gy		1.72±0.01	1.78±0.01	1.56±0.01	1.46±0.01	1.67±0.01	1.2±0.01
50-80 Gy	3.87±0.01*	2.49*;1.64 ±0.01	1.78; 1.81 ±0.01	1.44±0.01	1.47±0.01		1.08; 1.25;1.19† ±0.01
30 Gy			1.78±0.01				1.25±0.01

2.3. Model of large DNA loops

Chromosomal loops arrange chromosomes into micelle-like structures, or the DNA "factories," where gene transcription takes place (Münkel *et al.*, 1999; Marko & Siggia, 1997). The loops we simulate are different from the giant loops on Mbp scale hypothesized in the multi-loop-subcompartment model of DNA loops on the Mbp-Gbp scale (MLS) model (Münkel *et al.,* 1999). We do not model smaller loops (≈ 20 kbp) either, because they are below the lower limit of resolution of the PFGE experiment. The lower limit of the resolution in our model is the Kuhn length (de Gennes, 1979), which is based on the statistical properties of chromatin from 20 kbp to the 1 Mbp range. Since we determined this length as 2 kbp, it is, therefore, the size of a monomer in our RW.

We model the proposed loops on the scale of 120 kbp (Münkel *et al.*, 1999). In our model, each chromosome begins with a random stretch of 120 kbp, then 10 consecutive loops of the size 120 kbp are simulated, then goes the next stretch of 120 kbp of DNA and so on (Fig. 3b). It has been shown that the end-to-end distance between two loci (monomers) on DNA, separated by ℓ kbp, scales like an RW within a certain genomic size range. In (Münkel *et al.*, 1999) it is argued that there are two linear regimes for the end-to-end distance scaling, which can be explained away by assuming that under ~Mbp genomic sizes we have an underlying chromatin RW, and for distances above ~Mbp scale we have an RW of larger aggregates of chromatin, which are suspected to be "giant" loops (Sachs *et al.*, 1995; Münkel *et al.*, 1999; Marko & Siggia, 1997). In this work, we rely on data in Ref. (Münkel *et al.*, 1999) and assume that the loops are on average 120 kbp in length, and that there are about 10 such loops in a bundle called a polymer micelle (or rosette, Fig. 3b), with each micelle being separated by a run of chromatin of 120 kbp.

Our code simulates each loop by a brute force approach, *i.e*., no artificial rule to close a RW to form a loop is enforced. Each loop has 60 monomers. The first loop monomer is placed at a random (x,y,z) point inside the cell nucleus. The program creates an RW shooting in an arbitrary direction (Fig. 2). Then the RW evolves for 60 steps subject to volume restrictions imposed by the nucleus membrane and the chromosomal domains. If on the last step the RW does not return to the origin (x,y,z), it is discarded. Only when an RW is generated that closes onto itself can we say that it is a statistically unbiased loop and a thermally equilibrated one (Kremer & Grest, 1995). A collection of such loops is in thermal equilibrium, because no artificial restrictions were used to close RW onto themselves, besides the restriction of the nucleus membrane and the domain boundaries. Such simulation is very central processing unit (CPU) intensive, as a significant fraction of computational time is wasted to form a single loop.

2.4. Domain generation

The generated domains are spherical with some overlap allowed. Their volumes are proportional to the sizes of chromosomes. Each domain is checked for intersection with other domains, and this statistics is recorded. The x,y,z location of the center of a domain is simulated and placed randomly within the nucleus. However, domain centers cannot be too close to each other to provide for only partial overlap between domains. The diameter of each domain is calculated proportionately to the size of the corresponding chromosome. For instance, the domain for the first chromosome has the radius of 3.9 μm, while for chromosomes #46 the radius is only 2.3 μm. Forty-three percent of the nucleus volume is occupied by the domains. The domain center locations can change during the Monte-Carlo simulation, but the diameters remain the same.

2.5. The implementation of the numerical model

The DNAbreak model is now available as a part of the interface (NASARadiationTrackImage, copyright by Universities for Space Research Association (USRA)) written in Visual C++ 6.0, Visual FORTRAN 6.0, and OpenGL (open graphics library). This GUI is designed for experimentalists who will want to apply the model to their experimental data. All input data corresponding to experiments can be entered through dialogue boxes. The program used for DNA simulation, DNAbreak, was combined with Visual FORTRAN code previously employed by (Cucinotta *et al.,* 1995 and 1999). These tools are now combined into one master interface. Data from other models such as chromosomes domains and stochastic track structure (Nikjoo *et al.,* 2002a) can be input from data files. The GUI has three-dimensional (3D) displays of chromosomal domains, and will allow users to set up simulations through a single dialogue box that contains all parameters and options needed to set up the track properties, DNA and nucleus geometries, and experimental conditions. The track, the nucleus, the chromosomal domains, DNA loops, DSB (Fig. 3c), and chromosomes can be visualized through an OpenGL graphics window. This interface will help researchers to plan future experiments, and will be a reliable tool in predicting the outcome of envisioned experiments.

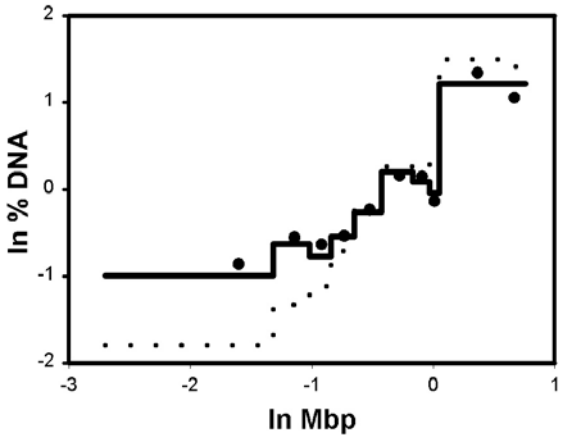

Figure 4. Comparison of the model to the data. The fragment-size distribution function (% DNA) is plotted vs. the fragment size in Mbp. Circles are experimental data (Höglund et al., 2000; human cells, N ions, dose=50 Gy, LET=225 keV/μm). The NASARadiationTrackImage model calculation is shown as a solid line. It fits data better than the random-breakage model (dotted line).

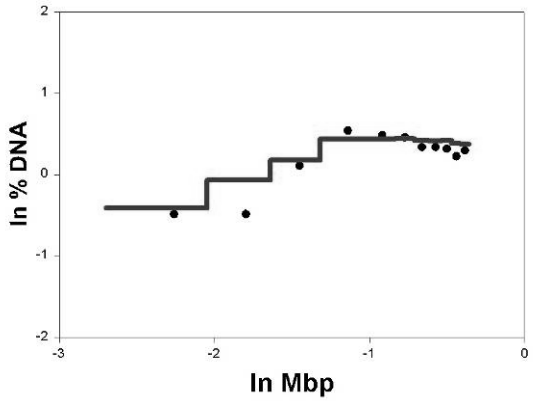

Figure 5. Comparison of the model to the data. The fragment-size distribution function (% DNA) is plotted vs. the fragment size in Mbp. Circles are PFGE data (Löbrich *et al*., 1996; human cells, Fe ions, dose=189 Gy, LET=151 keV/μm). The least-square fit obtained (the solid line) determines Q (=4.94x10^{-4} Gy^{-1}). The corresponding DSB cluster density is λ=0.224 Mbp^{-1}. The Fe ions are the most significant component of galactic cosmic rays (GCR), and will contribute the majority of DNA damage.

3. Results

3.1. Prediction of the fragment-size distribution function

Our model predicts the mass distribution of broken DNA fragments (Fig. 4). The graph shows, on a log-log scale, the mass fraction of a DNA pieces within a given size range vs. the average length of a fragment within this range. High-LET particles produce more relatively small DNA fragments, which is indicative of more concentrated and, therefore, less reparable biological damage. For instance, X rays would have produced fewer fragments on the left side of the graph. Here we show the good correspondence of the model data to the experiment, the quality of radiation to produce DNA fragments, Q (1/Gy), the average density of fragments per genomic length λ (1/Mbp), the yield of the DSBs, which are responsible for DNA fragmentation in # DSBs/Mbp/Gy units.

In Figs. 4 and 5 we give an example of NASARadiationTrackImage prediction of the fragment-size distribution function based on the χ^2-fitting of the experimental data. The model parameters are given in the figure captions. For comparison,

Table II. The estimated values for the DSB yields, #DSB/Mbp/Gy, are shown in a variety of experimental situations. Data from (Löbrich *et al.*, 1996((subscript[a]), and (Höglund *et al.*, 2000) (no subscript) were used. Optimizing DSB yields does not lead to very different values, indicating consistency between simulated data (DSB yields and the fragment-size distribution function) and experimental data. NASARadiationTrackImage-estimated DSB yields are recommended for high-LET radiation as more mechanistically justified.

DSByld x10^3	Fe, 150 keV/μm	N, 80-97 keV/μm	N, 125 keV/μm	N, 175 keV/μm	N, 225 keV/μm	He, 40 keV/μm	^{60}Co-photons <0.5 keV/μm
150-200 Gy	18.55[a]	12.3[a]; 8.5	9.05	7.15	7.05	9.15	6.0
100 Gy		8.6	8.9	7.8	7.3	8.35	6.0
50-80 Gy	19.35[a]	12.45[a]; 8.2	8.475	7.2	7.35		5.825
30 Gy			8.9				6.25

results of the random-breakage model are also given: the random-breakage model fails to give a useful prediction for the fragment-size distribution function of high-LET radiation. The discrepancy between the two distributions is less pronounced as LET decreases. The DSB yields for other simulations are summarized in Table II.

The yields did not differ by more than 5% from the previously estimated ones. However, we suggest the NASARadiationTrackImage model as a robust tool to estimate these yields, as the model was shown to produce high-quality fits for various LETs.

3.2. The dependence of the track efficiency parameter Q on dose and LET

The values of Q for a number of experimental situations are given in (Ponomarev *et al.*, 2001b). By the construction of the RLC formalism Q should be independent of dose. Intuitively, this can be seen from the fact that the DSB production efficiency of one track should not depend on whether other tracks are present. This property is confirmed from the numerical fits to the PFGE data (Figs. 4, 5).

3.3. Simulation of the Microbeam experiment with a fixed number of particles per cell

In this work our model was updated to include the simulation of an experiment with a fixed number of particles per cell, which we call here the simulation of the Microbeam experiment (Randers-Pehrson *et al.,* 2001). We intended to give a model representation of DNA breakage as it would occur in the Microbeam experiment. In the simulation, we choose a certain number of particles n hitting a cell with a randomly distributed impact parameter ρ, which originates from the imprecision of the particle collimator (Randers-Pehrson *et al.,* 2001). The focus of the beam is characterized by the parameter σ, which is the width at half maximum for the distribution of the impact parameter ρ. The number of tracks n can be any in our code, and in this work we demonstrate the results for situations with 1, 2, and 16 tracks per cell, which correspond to real experiments (Randers-Pehrson *et al.,* 2001; Sawant *et al.*, 2001). We used the Q values obtained from simulation of PFGE experiments (in Ponomarev *et al.* 2001b, and in Figs. 4, 5) with a homogenous radiation field and a fixed dose. The number of particles in those was *Poisson*-distributed in the plane perpendicular to the incident particles direction. Simulation of PFGE experiments calibrates Q, which allows us to predict fragment sizes for other situations, such as the case when one has a fixed number of particles per cell with a non-homogenous distribution of the impact parameter characterized by σ. We analyzed the theoretical data for their dependence on the most important parameters characterizing the quality of radiation and the geometry of DNA configuration in cell nucleus as well as the shape of the nucleus.

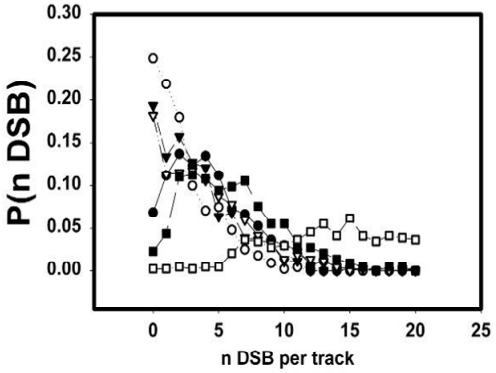

Figure 6. A track striking a cell, as it happens, for example, in a Microbeam experiment, can produce any number of DSBs with different probabilities. Too many DSBs are highly unlikely; on the other hand, no DSBs can have a sizable probability for not-so-high-LET particles such as 40-keV/μm α-particles. Other geometric factors influence this probability, as we can see from this figure. Each particle has its own most likely number of DSBs and its own average number of DSBs. This figure shows that high-LET 225 keV/μm N ions are more efficient in the production of DSBs (hollow squares), and that LET is the most important factor influencing the number of DSBs per track. The group of curves above the hollow cubes is the action of 40 keV/μm He particles. Hollow circle: flat nucleus (2:2:1/2 main axes ratio), defocused beam (σ=2.5 μm); filled triangles: round nucleus, defocused beam (σ=0.17 μm); hollow triangles: round nucleus, σ=2.5 μm, chromosomal domains imposed; filled rhombi: round nucleus, σ=0.17 μm; filled boxes: round nucleus, σ=0.17 μm, domains imposed. The curves show impact on the nucleus geometric parameters and other parameters on the efficiency of DSB formation. Flat nucleus hit by a moderate-LET α-particle has about 25% of "misses," or no DSB per track per cell (empty circles). A round nucleus and a focused beam setup result in a *Poisson*-like distribution of the number of DSBs with the maximum probability for 2–4 DSBs per track. The effect of domains is not detectable. The least important factor after the beam focus and the flatness of the nucleus is the effect of chromosomal domains.

Fig. 6 shows that LET is the most significant factor determining the shape of the number of DSBs per cell per track distribution, the shape of the nucleus is second, the impact parameter (the focus of the beam) third, and the presence of chromosomal domain is the least significant factor. We came to a conclusion that DSB production per cell per Gy is the same for a constant dose by different

LET. This agrees with the established fact that the DSB radio-biological efficiency (RBE) is almost LET-independent.

However, depending on LET, a single track can have a totally different impact on a cell. The average dose, based on the energy imparted to the nucleus volume, and averaged over that volume, depends on the type of incident particles. If one averages the energy imparted over the cell volume, one can calculate the action of an N ion particle at 255 keV/μm corresponds to a dose of 0.43 Gy (this is similar to the estimates of the dose delivered by a single Fe ion mentioned in the Introduction), and a 40-keV/μm α-particle corresponds to a dose of 0.08 Gy, both for σ=0.17 μm. A dose associated with one particle corresponds to the dose, as it is reported in an experiment with a random field of particles, if each cell gets one particle on average and the result is averaged over many cells and over cell volumes. Today technology allows irradiating a vast amount of cells, each in a similar manner (Randers-Pehrson *et al.*, 2001). The reason why the distribution of the number of induced DSBs in Fig. 6 is so much wider for 225-keV/μm N ions is that there are many more DSBs on average per particle per cell for this particular ion. The DSB yield per Mbp per Gy is about the same for all ions.

Fig. 6 shows that the particle LET has a significant impact on the distribution of the number of DSBs per particle per cell in a simulated Microbeam experiment. An important finding is that, for not so high LET, a particle hitting a cell does not necessarily produce a DSB. This is true, for example, with the He ions (the first point on each curve except the curve for N ions). We believe that this finding is important for the interpretation of the experiments, as we observe that, in 7% of all cells, no DNA breakage can be observed even if there is a direct hit by a 40-keV/μm α-particle. Higher-LET N ions lead to a practically nonexistent "no DSB situation" and a higher probability to have several DSBs per particle per cell. It has been asserted that heavy ions are not really "high-LET" radiation because of their wide penumbras, which sets the ratios of certain chromosome aberrations (Sachs *et al.*, 1997) to be different from high-LET predictions for this biological endpoint. We see from our numerical experiments that a heavy ion is more of a combination of high-LET radiation focused closer to the track core, and low-LET radiation in the penumbra that can extend beyond the nucleus. The overall effect is, however, a *non-Poisson* fragment-size distribution with higher clustering of DSBs within nucleus (Euclidian space) and along chromosomes (genomic dimension), as the radiation at the track center has the most significant effect.

3.4. Analysis of the impact of the chromosomal domains on DNA fragmentation

The simulated domains do not seem to have a large impact on the DSB distribution; this can be seen from Fig. 6. In Microbeam experiment simulations, we used our model to deduce data on the DSB number distribution that would be difficult to obtain experimentally because of the small number of DSBs produced. If one particle, such as a 225-keV/μm N ion or a 40-keV/μm α-particle, hits a nucleus, then 0, 1, or more DSBs can be produced. The higher LET, the less likely 0 DSB (no DSB) will be created. For higher LET particles, we should see a peak in the DSB number distribution for larger numbers of DSBs produced per cell per particle. The average number of DSBs per particle could be low (about 4 DSB for 40-keV/μm α-particle). Notice, however, that the overall DSB yield in our numerical experiment corresponds to the ones reported in (Kremer & Grest, 1995), which are 7.8–8.2×10^{-3} #DSB/Gy/Mbp. This correspondence follows from our calibration of the model (Figs. 3, 4). Reported DSB yields for higher fluences are not defined the same way as the DSB yields per particle per cell. Our model calculates the yield of #DSB/Gy/Mbp because we can calculate the average dose in the cell nucleus. For instance, one α-particle deposits a

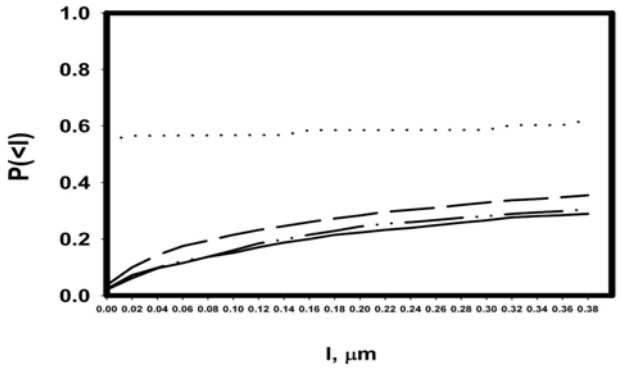

Figure 7. Cumulative probability of fragments of length <ℓ. The lengths shown correspond to only a fraction of all fragments. The DNA loops (dotted line, He 40 keV/μm) as seen from this figure will increase the frequency of shorter fragments in comparison to a simulation with no DNA loops (solid line). Higher LET (the dashed curve, 150-keV/μm Fe ions) leads to the same effect but to a smaller degree. This figure suggests that the effect of the DNA loops in combination with high-LET ions, such as 40-keV/μm He ions, is the prominent excess of short fragments (less than 0.05 μm in length). The dot-dashed line is the data for the same He ions, but in the DNA domains imposed. The domains do not have a significant influence on the number of small fragments.

small amount of energy on average corresponding to a dose of only about 0.08 Gy for a focused beam. The combination of the small dose and the small number of DSBs leads to a DSB yield (#DSB/Gy/Mbp) that is similar to the one reported in the experiment.

3.5. Geometric parameters controlling DNA breakage

The important conclusion that we can derive from Fig. 6 is that the DSB number distribution shows drastic change for higher LET, but for the same LET shows much smaller sensitivity to nucleus and DNA geometry. The curves for 40-keV/μm α-particles show that a flat nucleus would have a stronger impact on this distribution. The flat nucleus is defined as a disk with the smallest axis parallel to the direction of radiation (the principal axis ratio of the nucleus given by $ax^2 + by^2 + cz^2 = (6\mu m)^2$, is $x : y : z = \sqrt{\frac{1}{a} : \frac{1}{b} : \frac{1}{c}} = \sqrt{2 : 2 : \frac{1}{2}}$). We cannot make any conclusion on the degree of the influence that the presence of the chromosomal domains, or the change in the impact parameter σ, should have, because those effects are small and cannot be discerned even for high Monte-Carlo sampling (~20,000 samples). However, this is in an intuitive agreement because the chromosomal domains should only affect the locations of telomeres, which does not affect much the fragment-size distribution (Sachs *et al.*, 1999; Ponomarev & Cucinotta, 2006).

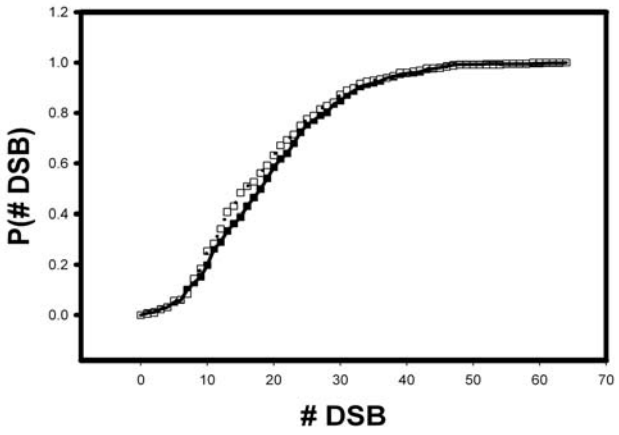

Panel A.

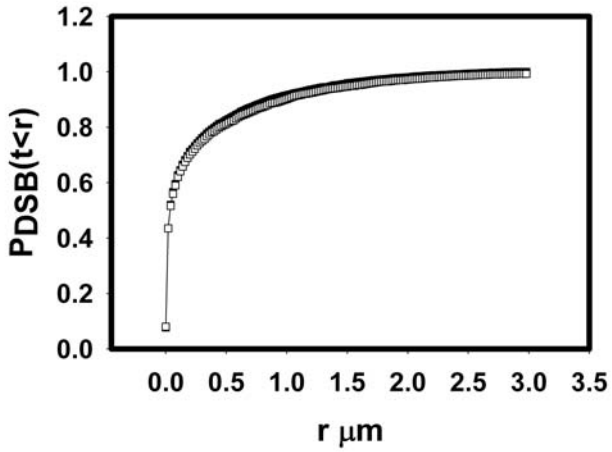

Panel B.

Figure 8. The simulated extent of the track penumbra. To make a single track simulation faster, a smaller cutoff on the extent of the track penumbra is beneficial. The cutoffs of 3 μm and 15 μm for 225-keV/μm N ions do not change significantly the cumulative DSB number distribution for one track per cell. The solid squares correspond to the cutoff of 3 μm and the hollow squares to the 15-μm cutoff (Panel A). Panel B is the data for the same ion and the same penumbra cutoffs (empty squares are 3 μm, and solid squares are 15 μm). Panel B shows the cumulative probability of a DSB to be anywhere at distance *t* not exceeding distance *r* in μm. Our choice of the cutoff parameters did not affect this probability. The cutoff of 5 μm was taken for other simulations as the optimal one.

3.6. The effect of loops

RW alone cannot account for the complexity of DNA organization in the cell nucleus. DNA loops have a strong impact on the number of small fragments (Fig. 7). The DNA loops lead to a preponderance of smaller fragments (Ponomarev *et al.*, 2006). This is in agreement with experimental work that points out that the high-order organization of DNA is accountable for the excess of the observed smaller DNA fragments (Radulescu *et al.*, 2004).

3.7. Justification of the penumbra cutoff

A numerical datum, in which the cutoff parameter for penumbra was varied with all other parameters constant, shows near-independence of the simulated track width. For N ions, the extent of the penumbra can be quite significant. The majority of numerical experiments were performed at the *cutoff*=5 μm, which is more than sufficient for narrow tracks of α-particles. Very large penumbra cutoffs will slow down the simulation, as we need to simulate the physical cylindrical space of the radius *Rp*+*Rc* (penumbra

plus cell nucleus). The sufficient extent of the penumbra cutoff was determined from a series of numerical experiments. We tested various cutoffs for N ions as their penumbra can extend up to 15 μm. However, for cutoffs of 3 and 15 μm, we have not noticed any systematic deviation for the number distribution of DSB in one track per cell experiment (Fig. 8). For all other data, the cutoff was 5 μm. The deviation between the simulated curves did not exceed the error of the numerical experiment. This is agreeable with the picture of drastic drop-off of energy distribution in ion tracks (Cucinotta *et al.* 1995 and 1999).

3.8. The effect of the track structure

The cumulative probability to have a DSB is shown as a function of a distance $\leq t$ from the track center (Fig. 9). This function is defined as a probability for a given DSB (regardless of the total number of DSBs) to be at a distance $\leq t$. Three cases are considered (1–3). DSB induction from 40-keV/μm He ions with (case 1) and without (case 2) DNA loops have same spatial pattern (two upper curves) of DSB formation. The DNA geometry has no impact on the DSB distribution in the Euclidian space (assuming DNA density is homogenous, but not necessarily constant, within the nucleus); only the track geometry does. DNA loops only influence fragment statistics, not the DSB location in the Euclidian space. The track structure for the 150-keV/μm Fe ions (case 3) is quite different from that of the He ions. DSB can form further from the track center for Fe ions than for He ions. The overall DNA damage from Fe ions is more spread out in the cell nucleus, even though the total number of DSBs per cell per track is higher (Table II). We found that He ions induce fewer DSBs but are more concentrated in the Euclidian space, while Fe ions induce more DSB, but some of them are more distant from the main grouping of DSBs.

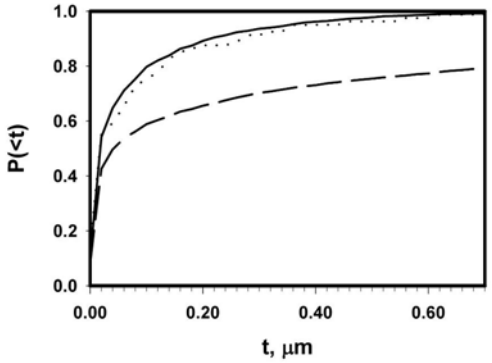

Figure 9. The cumulative probability to have a DSB at a distance $\leq t$ from the track center. This function is defined as a probability for one DSB, if such to occur from an ion, to be at a distance $\leq t$. Three cases are considered (1–3). DSB induction from 40-keV/μm He ions with (case 1) and without (case 2) DNA loop leads to the same spatial pattern (two upper curves). The track structure for 150-keV/μm Fe ions (case 3, no loops)) is quite different from He ions, as some DSBs can form further from the track center for Fe ions.

3.9. Q (the intensity parameter of the stochastic process of DSB formation) is independent of dose

Fig. 10 shows the values for the adjustable parameter Q as a function of dose. The numerical fits to experiments produce values for Q, which are, by and large, independent of dose. This is in agreement with the Eq. (4) that sets up the model, where the average number of DSBs per monomer is QD. The dependence on dose is already factored in through D, and Q should be dose-independent by definition. Fig. 10 shows this dose-independence, but indicates a slight dependence of this parameter on LET. High-LET particles are more efficient in DSB production per Gy than X rays.

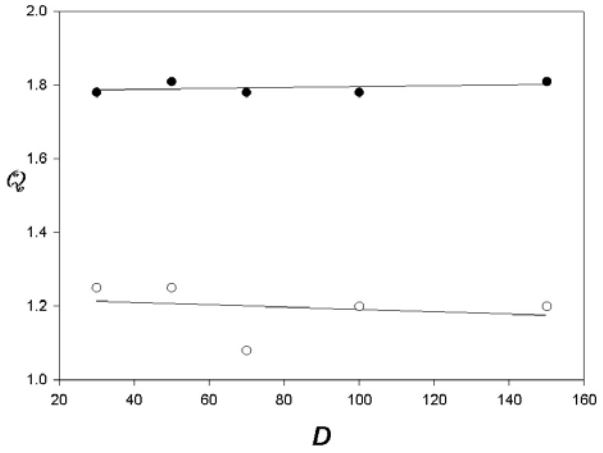

Figure 10. The intensity parameter of the DSB stochastic process Q vs. the dose of the PFGE experiment. This parameter is the only model's adjustable parameter defined in Eq. (4). The data are taken from Table I with the exact doses. This parameter determines Ψ, the probability per Gy to have a DSB at a monomer. In this work Q is determined by χ^2-fitting of the model to PFGE data, and is dose-independent as seen from this figure. For low-LET ^{60}Co photons this parameter is about 1.2 Gy^{-1} (open circles), and slightly higher for high-LET N ions (125 keV/μm, filled circles).

4. Conclusion

Our numerical model is now enhanced with chromosomal domains and DNA loops that are an essential component of the high-order DNA structure. The goal was to address the non-random distribution of 10–40 kbp fragments, for which these structures can play a role. We showed, however, that the chromosomal domains are not important for the specific biological endpoint of DNA fragmentation; but they certainly are important for other biological processes.

In our model, the whole nucleus with the human genome is constructed with large scale details of DNA organization. Simulation at this scale reduces our ability to address the smaller scale. Our limit of resolution was set at 2 kbp, below which our polymer model of DNA cannot discern the details of DNA breakage. The scale that we have addressed, however, overlaps the fragment ranges produced in the PFGE experiment.

Our model successfully predicts the distribution of larger DNA fragments and extrapolates data to lower doses and smaller fragment sizes. To account for a complex process of DSB formation in a small volume containing a small piece of DNA, a single adjustable parameter, Q, was used to generate a point process of DSB along the DNA arc length ℓ (Münkel *et al.,* 1999) with proper spatial and fragment-size distributions. The parameter Q is the intensity of the stochastic process of the DSB formation, and is the only adjustable parameter in the model that is determined by the model fits to the experimental data. We showed that the parameter Q only weakly depends on LET (Table I), which is consistent with the fact that DSB RBE is almost LET-independent. Our conclusion is that non-randomness in the DSB distribution resulting from high LET, and the clustering both in space and along DNA, is due to the superposition of DNA geometry and track geometry. This model takes into account two physical processes: a local process of DSB formation from a certain amount of incident energy in a small volume, as characterized by LET-insensitive parameter Q; and a global process of many DSB and correlations among them, determined by DNA and track geometry on a large scale.

The DSB yield in the model can either be determined from Q, or by a direct count of DSB in Monte-Carlo samples. Both numbers are very close to each other. The novelty of our approach is that the stochastic process generated with this parameter reproduces the clustering of DSB for high-LET and, therefore, provides a better suggested DSB yields than the ones proposed in (Stenerlöw *et al.,* 2003; Löbrich *et al.,* 1996; Höglund *et al.* 2000).

With the help of our formalism, we extrapolated the fragment statistics to size 0 by estimating the cumulative probability to have a fragment shorter or equal to the monomer size (2 kbp). In the code, the genomic distance on the lattice between two DSBs corresponding to ℓ<2 kbp is recorded as *f(0)*, where *f* is the fragment-size distribution function. *f(0)* has a finite value corresponding to all fragments of the size ℓ<2 kbp. This procedure is our workaround for the problem of missing fragment sizes in the PFGE experiment below the minimal fragment size, and adds the DSB count for such small fragments to obtain the total DSB yield. More detailed data for fragments smaller than 2 kbp are obtained by other researchers (Nikjoo *et al.,* 2002a). When the fragment-size distribution is determined for all sizes, the model predicts the DSB yield with higher precision than other models because the yield is based on a non-random DNA fragment distribution. As we noted, no significant discrepancy from the reported experimental DSB yields was found. We believe that this is due to the fact that high LET does not affect the DSB RBE, but it does affect the exact form of the fragment-size distribution.

The problem with the PFGE experiment (Stenerlöw *et al.,* 2003; Löbrich *et al.,* 1996; Höglund *et al.,* 2000) is that the data for small fragments (10–30 kbp) are absent due to limitations inherent in the experimental technique. The DSB yield can only be obtained from the fragment-size distribution function extrapolated for a wide range of sizes (from a few bp to ~Mbp). Experimentalists typically use the random breakage model for the extrapolation to smaller sizes. The random model, however, cannot account for high-LET effects in the case of HZE particles. Although our reported results did not show DSB yields noticeably different from the reported ones in experimental articles, the technique we propose is more consistent with the current knowledge of DNA organization and the track structure.

We have come to the following conclusions for the effect of DNA loops and the chromosomal domains on fragment sizes:

1) The chromosomal domains impose some topological restrictions on the location of telomeres within a cell nucleus and a limit on the mean square distance given between two monomers separated by a genomic distance ℓ. The presence of the nucleus membrane and domain borders changes the scaling law with which the mean square distance depends on ℓ. The square root of the mean square distance no longer linearly depends on ℓ, as it would for an unrestricted RW. This is observed in the ~Mbp region of genomic distances (Sachs *et al.,* 1995). This effect will

be vanishing for the small ℓ's (about 40 kbp and up to 1 Mbp) found with DNA fragments at high doses, especially from high-LET radiation. However, our conclusion is that the domains do not play any role in the fragment-size distribution function.

2) DNA loops on 120-kbp scale lead to an even more pronounced excess of smaller fragments in the 10–40-kbp range than predicted previously by the DNAbreak model (Ponomarev *et al.*, 2001a and 2001b). The presence of DNA loops does not affect the DSB yield. DNA loops should not affect the statistics of short fragments for low-LET radiation, such as X rays, as their homogenous radiation field leads to random breakage regardless how DNA is arranged.

3) Other conclusions are: The spatial distribution of DSB is not affected by the DNA organization at all; it only depends on the track structure. DNA fragment sizes do depend both on the track structure and the DNA organization. A flat nucleus, as it often occurs when cells are plated, resulted in a less severe DNA damage per track per cell. A defocused beam in the Microbeam experiment results in a less severe DNA damage per track per cell. α-particles with moderate LET can result in cells with no DSB induced, even after a direct hit, with a significant probability. High-LET ions, such as N ions and Fe ions, would always result in some breakage. High-LET ions produce more DSBs per track per cell, but DSBs are less concentrated around a line in the Euclidian space because of wider penumbra, while α-particles result almost in a needle-like action. That is, if there are several DSBs induced by an α-particle, they are almost always located along a line in Euclidian space.

The significance of our model is in its ability to predict the effects related not to the total number of DSB per Gy per cell but to their mutual locations in the nucleus. We showed how the spatial and genomic arrangements of DSBs are influenced by the loops and domains. The predicted effects will be important for the analysis of DNA repair and chromosomal aberrations.

5. References

Badhwar, G.D., Atwell, W., Badavi, F.F., Yang, T.C., and Cleghorn, T.F., Space Radiation Absorbed Dose Distribution in a Human Phantom. *Radiation Research* **157**, No. 1, 76–91, 2002.

Belli, M., Cherubini, R., Dalla Vecchia, M., Dini, V., Moschini, G., Simone, G., Tabocchini, M.A., Tiveron, P., DNA DSB induction and rejoining in V79 cells irradiated with light ions: a constant field get electrophoresis study. *Int. J. Radiat. Biol*. **76(8)**, 1095–1104, 2000.

Blöcher, D., In CHEF electrophoresis a linear induction of DSBs corresponds to a nonlinear fraction of extracted DNA with dose. *International Journal of Radiation Biology* **57**, 7–12, 1990.

Brandt, W., and Ritchie, R.H., Primary processes in the physical stage. *Physical Mechanisms in Radiation Biology* (R.D. Cooper, and R. Woods, Eds.), Tech. Info. Center, US, Atomic Energy Commission, Springfield, VA, 1974, pp. 20–29.

Brenner, D.J., Ward, J.F., Constraints on energy deposition and target size of multiply damaged sites associated with DNA double-strand breaks. *Int. J. Radiat. Biol*. **61**, 737–748, 1992.

Campa, A., Esposito, G., Belli, M., Simone, G., Tabocchini, M.A., DNA fragmentation in V79 cells irradiated with light ions as measured by pulsed-field gel electrophoresis. II. Simulation with a generalized broken stick model. *Int. J. Radiat. Biol.* **80(3)**, 229–238, 2004.

Cook, V.E., and Mortimer, R.K., A quantitative model of DNA fragments generated by ionizing radiation, and possible experimental applications. *Radiat. Res.* **125(1)**, 102–106, 1991.

Cucinotta, F.A., Katz, R., Wilson, J.W., Radial distribution of electron spectra from high-energy ions. *Radiat. Environ. Biophys.* **37(4)**, 259–265, 1998a.

Cucinotta, F.A., Katz, R., Wilson, J.W., Dubey, R.R., Radial dose distributions in the delta-ray theory of track structures. *Proceedings of two-center effects in ion-atom collisions, AIP Conference Proceedings* (T.J. Gray and A.F. Starace Eds.), Woodbury, NY, 1995, pp. 245–265.

Cucinotta, F.A., Nikjoo, H., and Goodhead, D.T., The effects of delta-rays on the number of particle-track traversals per cell in laboratory and space exposures. *Rad. Res*. **150**, 115–119, 1998b.

Cucinotta, F.A., Nikjoo, H., Goodhead, D.T., Applications of Amorphous Track Models in Radiation Biology. *Radiation and Environmental Biophysics* **38**, 81–92, 1999.

Cucinotta, F.A., Nikjoo, H., Goodhead, D.T., Model for Radial Dependence of Frequency Distributions for Energy Imparted in Nanometer Volumes from HZE Particles. *Radiation Research* **153(4)**, 459–468, 2000.

Cucinotta, F.A., Kim, M.Y., and Ren, L., Managing Lunar and Mars Mission Radiation Risks Part I: Cancer Risks, Uncertainties, and Shielding Effectiveness. NASA TP-2005-213164

de Gennes, P.-G., *Scaling Concepts in Polymer Physics*, Cornell University Press, Ithaca and London, 1979, p. 31.

Ernest Orlando Lawrence Berkeley National Laboratory, LBL. Report Number: LBNL-40278. Modeling Human Risk: Cell & Molecular Biology in Context. University of California, Berkeley, CA 94720, Jun. 1997.

Goodhead, D.T., Molecular and cell models of biological effects of heavy ion radiation. *Radiat. Environ. Biophys*. **34**, 67–72, 1995.

Höglund, E., Blomquist, E., Carlsson, J., Stenerlöw, B., DNA damage induced by radiation of different linear energy transfer: initial fragmentation. *Int. J. Radiat. Biol*. **76(4)**, 539–547, 2000.

Kobetich, E.J., and Katz, R., Energy deposition by electron beams and γ-rays. *Phys. Rev.* **170**, 257–265, 1969.

Kremer, K., Grest, G.., Entanglement effects in polymer melts and networks. *Monte Carlo and Molecular Dynamics Simulations in Polymer Science*, edited by K. Binder. New York, Oxford: Oxford University Press, 1995, pp. 194–271.

Laughton, G.A., Grindon, C., Girard, P., Nikjoo, H., The Mysteries of Telomere Structure and Recognition: could Radioprobing Help*? Int. J. Radiat. Biol*. **80(11-12)**, 805–811, 2004.

Löbrich, M., Cooper, P.K., Rydberg, B., Non-random distribution of DNA double-strand breaks induced by particle irradiation. *Int. J. Radiat. Biol*. **70**, 493–503, 1996.

Marko, J.F., Siggia, E.D., Polymer models of meiotic and mitotic chromosomes. *Mol. Biol. Cell* **8(11)**, 2217–2231, 1997.

Münkel, C., Eils, R., Dietzel, S., Zink, D., Mehring, C., Wedemann, G., Cremer, T., Langowski, J., Compartmentalization of interphase chromosomes observed in simulation and experiment. *J. Mol. Biol*. **285(3)**, 1053–1065, 1999.

National Council of Radiation Protection and Measurements, NCRP. Guidance on Radiation Received in Space Activities. NCRP Report 98, Bethesda, MD, 1989.

Newman, H.C., Prise, K.M., Folkard, M., Michael, B.D., DNA double-strand break distributions in X-ray and alpha-particle irradiated V79 cells: evidence for non-random breakage. *Int. J. Radiat. Biol.* **71**, 347-63, 1997.

Nikjoo, H., Bolton, C.E., Watanabe, R., Terissol, M., O'Neill, P., Goodhead, D.T., Modeling of DNA damage induced by energetic electrons (100 eV to 100 keV). *Radiat. Prot. Dosimetry* **99(1-4)**, 77–80, 2002a.

Nikjoo, H., Khvostunov, I.K., Cucinotta, F.A., The Response of Tissue-Equivalent Proportional Counters to Heavy Ions. *Radiation Research* **157**, 435–445, 2002b.

Pinto, M., Prise, K.M., Michael, B.D., A Monte Carlo model of DNA double-strand break clustering and rejoining kinetics for the analysis of pulsed-field gel electrophoresis data. *Radiat. Res.* **162(4)**, 453–463, 2004.

Ponomarev, A.L., Brenner, D.J., Hlatky, L.R., Sachs, R.K., A Polymer, Random-Walk Model for the Size-Distribution of Large DNA Fragments after High-LET Radiation. *Radiation and Environmental Biophysics* **39(2)**, 111-120, 2000.

Ponomarev, A.L., Cucinotta, F.A., Chromatin loops are responsible for higher counts of small DNA fragments induced by high-LET radiation, while chromosomal domains do not affect the fragment sizes. *International Journal of Radiation Biology*, in press, 2006.

Ponomarev, A.L., Sachs, R.K., Polymer Chromosome Models and Monte-Carlo Simulations of Radiation Breaking DNA. *Bioinformatics* **15(12)**, 957–964, 1999; code available at http://www.math.berkeley.edu/~sachs.

Prise, K.M., Ionizing Radiation Induced Clustered Damage to DNA - A Review of the Experimental Evidence. *Microdosimetry: An Interdisciplinary Approach* (D.T. Goodhead, P. O'Neill and H.G. Menzel, Eds.), Royal Society of Chemistry, Cambridge, UK, 1997, pp. 111–116.

Radulescu, I., Elmroth, K., Stenerlöw, B., Chromatin Organization Contributes to Non-randomly Distributed Double-Strand Breaks after Exposure to High-LET Radiation. *Radiation Research* **161**, 1–8, 2004.

Randers-Pehrson, G., Geard, C.R., Johnson, G., Elliston, C.D., Brenner, D.J., The Columbia University Single-Ion Microbeam. *Radiation Research* **156**, 210–214, 2001.

Rogakou, E.P., Pilch, D.R., Orr, A.H., Ivanova, V.S., and Bonner, W.M., DNA double-stranded breaks induce histone H2AX phosphorylation on serine 139. *J. Biol. Chem*. **273**, 5858–5868, 1998.

Rothkamm, K., and Löbrich, M., Evidence for a lack of DNA double-strand break repair in human cells exposed to very low x-ray doses. *Proc. Natl. Acad. Sci. USA* **100(9)**, 5057–5062, 2003.

Sachs, R.K., Brenner, D.J., Chen, A.M., Hahnfeldt, P., Hlatky, L.R., Intra-arm and interarm chromosome intrachanges: tools for probing the geometry and dynamics of chromatin. *Radiat. Res.* **148(4)**, 330–340, 1997.

Sachs, R.K., Hahnfeldt, P.J., Ponomarev, A.L., Hlatky, L.R., Genomic locations of radiation-produced DNA double strand breaks: a stochastic cluster process formalism. *Math. Biosciences* **159**, 165–87, 1999.

Sachs, R.K., Yokota, H., van-den-Engh, G., Trask, B., Hearst, J.E., A random-walk/giant loop model for interphase chromosomes. *Proc. Nat. Acad. Sci. U.S.* **92**, 2710–2714, 1995.

Sawant, S.G., Randers-Pehrson, G., Geard, C.R., Brenner, D.J., Hall, E.J., The bystander effect in radiation oncogenesis: I. Transformation in C3H 10T1/2 cells in vitro can be initiated in the unirradiated neighbors of irradiated cells. *Radiat. Res.* **155(3)**, Mar. 2001, pp. 397–401.

Stenerlöw, B., Karlsson, K.H., Cooper, B., Rydberg, B., Measurement of Prompt DNA Double-Strand Breaks in Mammalian Cells without Including Heat-Labile Sites: Results for Cells Deficient in Nonhomologous End Joining. *Radiation Research* **159**, 502–510, 2003.

Taucher-Scholz, G., Immediate localized CDKN1A (p21) radiation response after damage produced by heavy-Ion tracks. *Radiat. Res*. **154(4)**, 398–405, 2000.

Townsend, L.W., Cucinotta, F.A., and Wilson, J.W., Interplanetary crew exposure estimates for galactic cosmic rays. *Radiat. Res*. **129**, 48–52, 1992.

Turner, N.D., Braby, L.A., Ford, J., and Lupton, J.R., Opportunities for nutritional amelioration of radiation-induced cellular damage. *Nutrition* **18**, 904-912, 2002.

Wilson, J.W., Townsend, L.W., and Badavi, F.F., Galactic HZE propagation through the Earth's atmosphere. *Radiat. Res*. **109**, 173–183, 1987.

Wu, H., Durante, M., George, K., Goodwin, E.H., Yang, T.C., Rejoining and Misrejoining of Radiation-Induced Chromatin Breaks. II. Biophysical Model. *Radiation Research* **145**, 281–288, 1996.

REPORT DOCUMENTATION PAGE

Form Approved
OMB No. 0704-0188

1. AGENCY USE ONLY *(Leave Blank)*	2. REPORT DATE	3. REPORT TYPE AND DATES COVERED
	May 2006	NASA Technical Paper

4. TITLE AND SUBTITLE
NASA Radiation Track Image GUI for Assessing Space Radiation Biological Effects

5. FUNDING NUMBERS

6. AUTHOR(S)
Artem L. Ponomarev
Francis A. Cucinotta

7. PERFORMING ORGANIZATION NAME(S) AND ADDRESS(ES)
Johnson Space Center

8. PERFORMING ORGANIZATION REPORT NUMBERS
S-976

9. SPONSORING/MONITORING AGENCY NAME(S) AND ADDRESS(ES)
National Aeronautics and Space Administration
Washington, DC 20546-0001

10. SPONSORING/MONITORING AGENCY REPORT NUMBER
TP-2006-213719

11. SUPPLEMENTARY NOTES

12a. DISTRIBUTION/AVAILABILITY STATEMENT
Unclassified/Unlimited
Available from the NASA Center for AeroSpace Information (CASI)
7121 Standard
Hanover, MD 21076-1320 Category: 52

12b. DISTRIBUTION CODE

13. ABSTRACT *(Maximum 200 words)*

The high-charge high-energy (HZE) ion components of the galactic cosmic rays when compared to terrestrial forms of radiations present unique challenges to biological systems. In this paper we present a deoxyribonucleic acid (DNA) breakage model to visualize and analyze the impact of chromatin domains and DNA loops on clustering of DNA damage from X rays, protons, and HZE ions. Our model of DNA breakage is based on a stochastic process of DNA double-strand break (DSB) formulation that includes the amorphous model of the radiation track and a polymer model of DNA packed in the cell nucleus. Our model is a Monte-Carlo simulation based on a randomnly located DSB cluster formulation that accomodates both high- and low-linear energy transfer radiations. We demonstrate that HZE ions have a strong impact on DSB clustering, both along the chromosome length and in the nucleus volume. The effects of chromosomal domains and DNA loops on the DSB fragment-size distribution and the spatial distribution of DSB in the nucleus were studied. We compare our model predictions with the spatial distribution of DSB obtained from experiments. The implications of our model predictions for radiation protection are discussed.

14. SUBJECT TERMS	15. NUMBER OF PAGES	16. PRICE CODE
galactic cosmic rays; terrestrial radiation; deoxyribonucleic acid; simulation; energy transfer; chromosomes; ions; models	30	

17. SECURITY CLASSIFICATION OF REPORT	18. SECURITY CLASSIFICATION OF THIS PAGE	19. SECURITY CLASSIFICATION OF ABSTRACT	20. LIMITATION OF ABSTRACT
Unclassified	Unclassified	Unlimited	Unlimited